

Transition from Thermal to Recombining Plasma in a Free Expanding Arc Jet Plasma Generator

Shinichi NAMBA, Keisuke NAKAMURA, Noriyasu YASHIO,
Shinya FURUKAWA, Ken TAKIYAMA

Graduate School of Engineering, Hiroshima University, 1-4-1 Higashi-Hiroshima, Hiroshima 739-8527 JAPAN

Kuninori SATO

National Institute for Fusion Science, 322-6 Oroshi-cyo, Toki, Gifu 509-5292 JAPAN

(Received: 8 September 2008 / Accepted: 7 November 2008)

A compact stationary arc jet plasma generator was constructed for fundamental research. The plasmas were produced with two shapes of anode nozzle having different diverging angle. Characterization of plasma parameters in the expanding helium plasmas was performed using a high resolution visible spectrometer. The plasma density and its temperature around the anode nozzle exit were evaluated by analysis of the spectral intensity and profile. In addition, it was found that the anode with the large diverging angle provided a favorable condition to generate a strong non-equilibrium recombining plasma. On the other hand, the expansion dynamics from the anode nozzle was also examined by a shadow graph method.

Keywords: arc jet plasma, thermal plasma, recombination plasma, plasma spectroscopy

1. Introduction

Thermal plasmas have attracted a great deal of interest for applications in various engineering and scientific fields [1] such as welding [2], nanoparticle synthesis [3], and waste treatment [4].

Thermal arc plasmas expanding through a converging and diverging nozzle with Laval or conical shape have also been expected to be one of the candidates for plasma thrusters [5]. For example, micropropulsion devices have been developed for orbital and attitude control of a small satellite so far. The small arc jet thruster has an advantage in its simple structure and compactness. In order to demonstrate the microplasma thruster, Horisawa *et al* examined the feasibility of DC arc jet operation at very low-power level [6]. However, as for characteristics of the plasma parameters only the gas temperature of propellant nitrogen gas was evaluated by spectroscopic observation. For the realization of the microthrusters, a comprehensive understanding of characteristics of the arc jet plasma generated is essential.

On the other hand, atomic and molecular processes in high-density, low-temperature recombination plasmas have also been studied extensively in arc jet plasmas. Indeed, a stationary population inversion between excited levels of neutral helium (He) was observed [7, 8]. Moreover, a formation of inverted population of the excited states of He⁺ ion, which is capable of producing a

lasing action for a vacuum ultraviolet (VUV) laser, has been demonstrated so far [9].

The high-density recombining plasma is also expected to play an important role in radiation cooling of high-heat flux plasma in a divertor region of nuclear fusion device [10], where He ash associated with DT fusion reaction will be exhausted. Since the divertor plate would be exposed to significant high-heat flux, several tens MW/m², the reduction of the heat load into plasma facing components is an urgent issue [11, 12].

Recently, we have developed a compact stationary arc jet plasma source for the purpose of the fundamental research on arc jet thrusters and atomic and molecular physics in plasmas. In order to characterize the arc jet plasma and evaluate plasma parameters, the spectroscopic observations were made using a high resolution visible spectrometer. Moreover, the dynamics of the plasma expanding from the anode nozzle was investigated by a shadow graph imaging method.

2. Experimental Setup

Figure 1(a) shows the schematic diagram of an expanding arc jet generator developed in this study. Stationary He arc plasmas were generated between an anode (copper) and a cathode (cerium tungsten: Ce/W). Both electrodes were cooled by water to prevent them from being damaged due to high-heat flux arc. The arc discharge

author's e-mail: namba@hiroshima-u.ac.jp

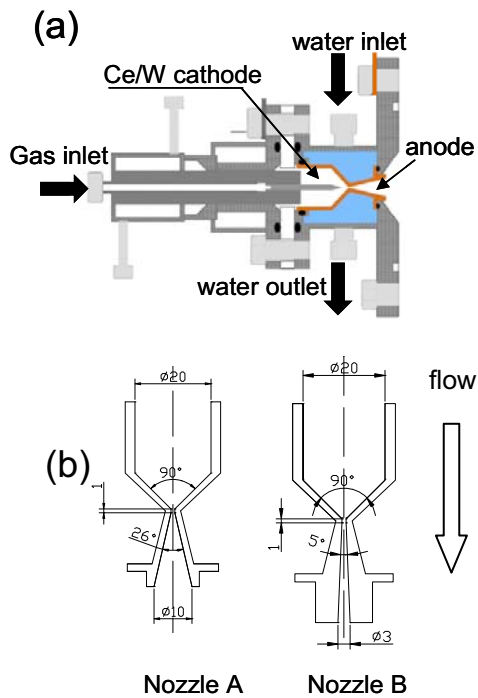


Fig. 1 Schematic diagram of the arc jet plasma source (a). The details of the anode nozzle A and B are shown in (b).

current and voltage were up to 200 A and ~ 20 V, respectively. The electrode gap length was 1 mm and the pressure at the discharge section was 1–1.4 atm. The typical discharge current was 70 A and discharge pressure was ~ 1.2 atm. In general, the arc plasma chokes the anode nozzle (throat diameter: 1.0 mm ϕ , constrictor length: 1.0 mm) and a plasma plugging effect due to its strong viscosity results in a large pressure gradient between the arc discharge section and expansion region. According to the hydrodynamic theory, the high enthalpy gas generated by the arc discharge is converted into the directional kinetic energy due to an adiabatic free expansion into vacuum. Thus, the parallel velocity component with respect to the expansion axis increases, while the perpendicular thermal motion is frozen rapidly. Subsequently, the atmospheric thermal plasma having a temperature of a few eV and a density of $10^{16}\sim 10^{17}$ cm $^{-3}$ turns into a rapid cooling plasma. Since the structure of converging and diverging nozzle significantly influences the adiabatic expansion, two shapes of the anode nozzle were employed in this study. Figure 1(b) shows the schematics of the two anodes. Nozzle A had a diverging angle of 26 $^\circ$ and exit diameter of 10 mm ϕ , while for nozzle B smaller angle and diameter of 5 $^\circ$ and 3 mm ϕ , respectively.

Spectroscopic observations were carried out using a high resolution visible spectrometer ($f = 1$ m, grating: 2400 grooves/mm) with a charge coupled device (CCD) camera and a photomultiplier tube. The emission measurements were made from both perpendicular and parallel to the

plasma expansion axis using an UV grade optical fiber. The resolution of the optical system was around 6 pm (the half width at half maximum: HWHM) for the CCD detection under an entrance slit width of 30 μ m. Relative spectral sensitivity of the whole optical system was calibrated by a standard tungsten ribbon lamp.

On the other hand, the dynamic behavior of high-heat flux plasma immediately after expansion from the anode nozzle was visualized by a standard shadow graph method using a He-Ne laser. We could not directly observe the anode nozzle exit itself from the perpendicular direction to the axis because of the restriction of the observation window. To this end, the arc discharge section was disconnected from the vacuum chamber and the imaging measurement was made only for the plasma expansion into the atmosphere. Since the pressure gradient between the plasma generation (1.2 atm) and expansion regions became small, the adiabatic expansion would, to some extent, be suppressed compared with that into vacuum.

3. Results and Discussion

3.1 Characterization of plasma parameters

The relatively high temperature (a few eV) and high density of $10^{16}\sim 10^{17}$ cm $^{-3}$ thermal plasmas were generated between the cathode and the anode electrodes due to the arc discharge. In order to characterize the plasma parameters of expanding arc jet at the initial stage, first the intense emission at the exit of nozzle B was observed from the parallel direction to the expansion axis. Figure 2 shows the He I 667.8 nm line emission (transition: $2p\ ^1P-3d\ ^1D$) along the line of sight, indicating the prominent line broadening. Again, note that the instrumental width was estimated to be ~ 6 pm (HWHM). Generally, the spectral line profile is given by the Voigt function consisted of Lorentzian shape due to pressure broadening (resonance and the Stark) and Gaussian (the Doppler and instrumental width) [13, 14]. The best fitted Voigt function is also represented in Fig. 2 with a solid curve. In the present study, the resonance broadening can be neglected because the gas temperature was sufficiently

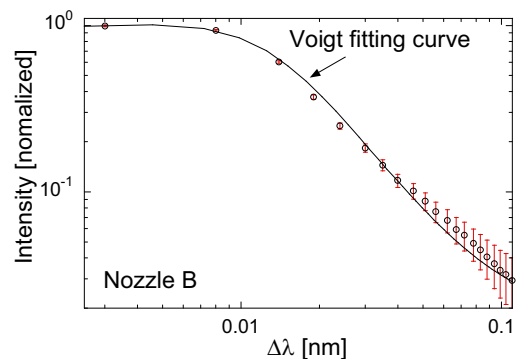


Fig. 2 Line spectrum of neutral He 667.8 nm at the exit of nozzle B. The Voigt fitting curve is also shown in a solid line.

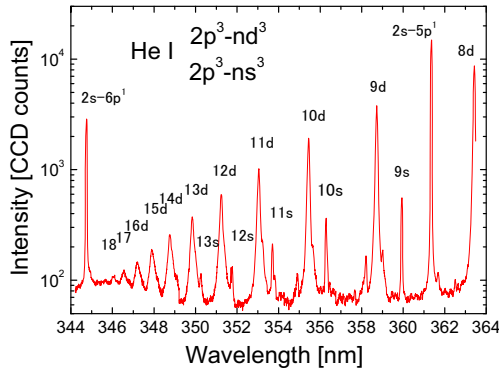


Fig. 3 The Rydberg spectra of He I $2p^3P\text{-}n^3D$ and $2p^3P\text{-}n^3S$ series and radiative recombination continuum spectra observed with nozzle A.

high [14]. Assuming that the Gaussian width ($T_i=0.3$ eV, see later) was 10 pm (HWHM), we obtain the Lorentzian width of ~ 13 pm (HWHM), corresponding to the electron density of $\sim 2 \times 10^{15}$ cm^{-3} at the nozzle exit [13]. For nozzle A, however, the spectral width was not broadened significantly, because the diverging angle and exit diameter of nozzle A were around three times larger than those of B. Thus, we estimate the plasma density by using an alternative method for nozzle A (see later).

Figure 3 shows the spectra attributed to He I $2p^3P\text{-}n^3D$ and $2p^3P\text{-}n^3S$ series observed for nozzle A at 45 mm downstream from the anode nozzle exit (perpendicular measurements to the jet axis). Line spectrum up to $n=18$ and radiative continuum spectra were observed, indicating the typical characteristics of the non-equilibrium recombining plasma, in which the three body recombination dominates the other atomic processes [7, 8]. Although for nozzle B the emissions up to $n=16$ were observable, the recombination continuum was absent. Moreover, for nozzle B the length of the plasma was over 700 mm and the column diameter was less than 10 mm at 45 mm from the nozzle, while for nozzle A the

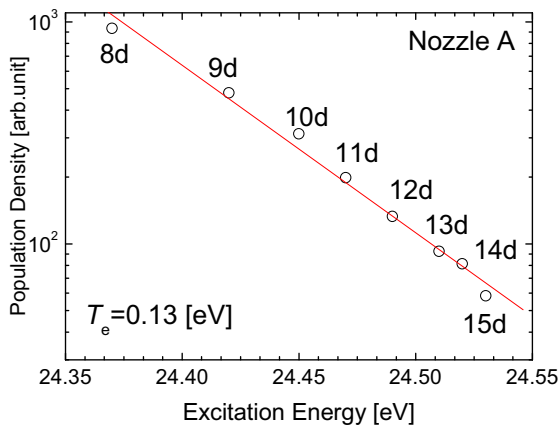


Fig. 4 The Boltzmann plot of $2p^3P\text{-}n^3D$ series for nozzle A. The straight line represents the temperature of 0.13 eV.

plasma radiated the bright emission immediately after the expansion from the nozzle and its length and diameter were less than 300 mm and ~ 30 mm, respectively. The difference in emission spectra between the two nozzles could be ascribed to particle collisions of the expanding plasma with residual He gas [7-9]. Since the flow conductance for nozzle A was higher than that for nozzle B due to the large diverging nozzle angle, the ambient gas pressure in the expansion region was high compared with the value of nozzle B. For nozzle A, the residual He atoms, therefore, could make the ejected plasma cool more rapidly due to elastic and inelastic collisions, which is mainly responsible for the production of strong non-equilibrium recombination plasma. Although for nozzle B the recombining plasma could also be generated, the collisional relaxation time between the electrons and the other particles should be longer than that of nozzle A, resulting in the low degree non-equilibrium recombining plasma [15].

The electron temperature in the recombining phase was determined by the population densities of excited states [16] in which local thermodynamic equilibrium (LTE) can be established among highly-excited levels. Thus, the distribution of population density of n^3D levels follows the Boltzmann's law. Figure 4 shows the Boltzmann plot evaluated from the $2p^3P\text{-}n^3D$ line intensities for nozzle A (FIG. 3). Here, since the spectral shapes were broadened by the Stark effect, especially, for higher levels, the deconvolution procedure was necessary for an accurate estimation of the spectral intensity, yielding the relevant population density. The straight line gives the electron temperature of $T_e = 0.13$ eV, indicating the production of low temperature plasma as expected. A similar electron temperature was also obtained for nozzle B, because the perpendicular temperature derived is considered to be determined by the hydrodynamic expansions rather than the processes on atomic physics.

As mentioned above, the radiative recombination

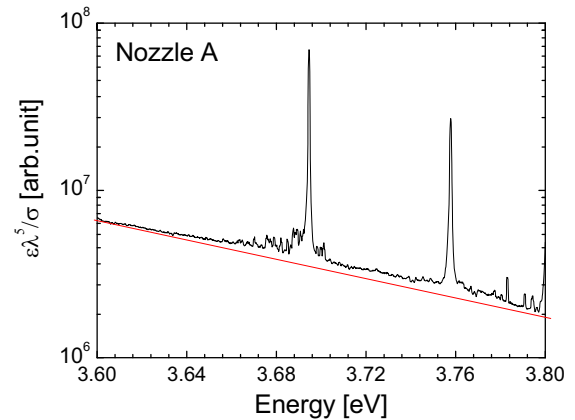


Fig. 5 Recombination continuum spectra terminated to $2p^3P$ (nozzle A). The straight line represents the electron temperature of $T_e=0.33$ eV.

continuum terminated to $2p\ ^3P$ transition, that is, $\text{He}^+ + e \rightarrow \text{He}^* (2p\ ^3P) + h\nu$, was also observed for nozzle A, where the strong recombining plasma was generated. The emission coefficient $\varepsilon(\lambda)$ relevant to this recombination is given by the following equation in the unit of $\text{erg/s/cm}^3/\text{sr/cm}(\text{wavelength})$ [17],

$$\varepsilon(\lambda) = \frac{h^7}{8\pi^{9/2}m^3e^6} \frac{c^2}{\lambda^5} \frac{g}{g_z} \sigma n_e n_z \left(\frac{E_H}{k_B T_e} \right)^{3/2} \exp \left[\frac{1}{k_B T_e} \left(\chi - \frac{ch}{\lambda} \right) \right], \quad (1)$$

where g and g_z are the statistical weights of the ground state of He atom and H-like ion (He^+), respectively, λ is the wavelength of continuum spectra, σ is the photo-ionization cross section for the ground state of He atom, E_H is the ionization energy of hydrogen, and χ is the ionization energy from He atom ground state. Figure 5 shows the plot of $\varepsilon(\lambda)\lambda^5/\sigma$ on the excitation energy. The best fitted curve which corresponds to $T_e=0.33$ eV is also represented in the figure. The temperature obtained by continuum spectra is not in good agreement with the value evaluated by the Boltzmann plot. This could be interpreted by that the population densities of highly-lying levels were not estimated accurately by the deconvolution procedure due to the line merging with the neighboring transitions, resulting in the underestimation of the electron temperature.

On the other hand, since the spectral broadening width for nozzle A was not sufficient to estimate the density as described before, an alternative method was employed in this study. According to Inglis-Teller relationship, the electron density can be expressed by,

$$\log n_e = 23.491 - 1.5 \log |Z_p| + 4.5 \log Z - 7.7 \log n_m, \quad (2)$$

where Z_p is the charge and Z is the atomic number [18]. The value n_m is the resolvable maximum quantum number. For nozzle A, the n_m was 18, as shown in FIG. 3. By substituting the parameters into Eq. (2), we obtain the density of $\sim 3 \times 10^{13} \text{ cm}^{-3}$ at 45 mm from the nozzle.

Finally, the flow velocity of the arc jet plasma was determined by measuring the Doppler shift of He I 667.8 nm in the perpendicular and parallel to the expansion axis. The blue shift observed in the parallel direction was 63.4 pm, corresponding to the flow speed of 2.7×10^4 m/s. Assuming that the thermal plasma ejected from the anode nozzle reaches the terminal velocity, we obtain the temperature of ~ 6.1 eV at the arc discharge section.

3.2 Visualization of expanding plasmas

The plasma expansion behavior immediately after ejected from the anode nozzle was examined by a shadow graph method. Figure 6 shows an image of the plasma flow for nozzle B. The diverging angle of the anode nozzle is also depicted in the figure. As clearly seen, the radius of the plasma column was similar to that of the

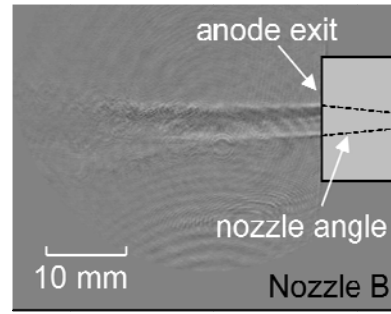


Fig. 6 Shadow graph image of expanding plasma from the anode nozzle B.

nozzle exit over the length of ~ 20 mm. This implies that thermal pinch effect due to an interaction of the expanding plasma with the anode nozzle wall could cause the arc temperature at the column axis increased [19]. Thus, the arc plasma jet with a narrow divergence was obtained for nozzle B. On the other hand, for nozzle A the flow structure was not observed. Since the pinch could be less effective due to the larger expansion angle, we have concluded that the density gradient of the plasma was not sufficiently high to record the flow image.

4. Summary

We developed a compact arc jet plasma generator, and the characterizations of He arc jet plasmas generated using two shapes of the anode nozzle were accomplished with high spectral resolution visible spectroscopy. For the large diverging angle nozzle, it was found that the plasma recombination was promoted significantly due to particle collision with the ambient gas and turned into the non-equilibrium recombining plasma with the temperature of ~ 0.3 eV. On the other hand, it was considered that the rapid cooling for the nozzle with narrow angle was less effective. In addition, the measurement of the Doppler shift yielded that the plasma flow speed was very high ($\sim 2.7 \times 10^4$ m/s) and the initial temperature of the arc plasma section was evaluated to be as high as ~ 6 eV.

Furthermore, the shadow graph imaging showed that the thermal pinch effect came into play for nozzle B with the narrower diverging angle and smaller exit diameter, resulting in the high-density gradient and successful visualizations of the plasma flow.

Acknowledgements

We would like to thank H. Akatsuka (Tokyo Institute of Technology) and K. Ono (Kyoto University) for helpful discussions to construct and design the compact arc plasma generator. This work is performed with the support and under the auspices of the NIFS Collaborative Research Program.

- [1] M. I. Boulos, P. Fauchais and E. Pfender, *Thermal Plasmas: Fundamentals and Applications* (Plenum, 1994).
- [2] B. C. Howard and S. C. Helzer, *Modern Welding Technology* (Welding Prentice Hall College Div, 2004).
- [3] N. Rao, S. Girshick, J. Hebelein, P. McMurry, S. Jones, D. Hansen and B. Micheel, *Plasma Chemistry and Plasma Processing*, **15**, 581 (2005).
- [4] T. Inaba, T. Iwao, *IEEE Trans. Dielectr. Electr. Insul.* **7**, 684 (2000).
- [5] E. Choueiri ed., *Physics of Plasma Propulsion*, (CRC press, 2007).
- [6] H. Hiroshima and I. Kimura, *Vacuum* **59**, 106 (2000).
- [7] H. Akatsuka and M. Suzuki, *Phys. Rev. E*, **49**, 1534 (1994).
- [8] S. Namba, M. Goto, H. Tsuboi, T. Oda, K. Sato, *J. Appl. Phys.* **88**, 3182 (2000).
- [9] K. Sato, M. Shiho, M. Hosokawa, H. Sugawara, T. Oda and T. Sasaki, *Phys. Rev. Lett.* **39**, 1074 (1977).
- [10] T. W. Petrie, R. Maingi, S. L. Allen, D. A. Buchenauer, D. N. Hill and C. J. Lasnier, *Nucl. Fusion*, **37**, 643 (1997).
- [11] R. Parker, G. Janeschitz, H. D. Pacher, D. Post, S. Chiocchio, G. Federici, P. Ladd, and ITER, Joint Central Team, Home Teams, *J. Nucl. Mater.* **241–243**, 1 (1997).
- [12] G. Janeschitz, K. Borrass, C. Federici, Y. Igitkhanov, A. Kukushukin, H. D. Pacher, G. W. Pacher, and M. Sugihara, *J. Nucl. Mater.* **220–222**, 73 (1995).
- [13] R. W. P. McWhirter, in *Plasma Diagnostic Techniques*, edited by R. H. Huddlestone and S. L. Leonard (Academic, New York, 1965).
- [14] H. R. Griem, *Spectral Line Broadening by Plasmas* (Academic, New York, 1974).
- [15] S. Byron, R. C. Stabler, and P. I. Bortz, *Phys. Rev. Lett.* **8**, 376 (1962).
- [16] W. Lochte-Holtgreven ed, *Plasma Diagnostics* (Elsevier Science, 1968).
- [17] M. Otsuka, R. Ikee, and K. Ishii, *J. Quant. Spectrosc. Radiat. Transf.* **15**, 995 (1975).
- [18] D. R. Inglis and E. Teller, *Astrophys. J.* **90**, 439 (1939).
- [19] S. Greenfield, I. L. Jones and C. T. Berry, *Analyst*, **89**, 713 (1964).